Physics of the Earth and Planetary Interiors 176 (2009) 33–43

Contents lists available at ScienceDirect

Physics of the Earth and Planetary Interiors

journal homepage: www.elsevier.com/locate/pepi

Upper mantle anisotropy beneath Indochina block and adjacent regions from shear-wave splitting analysis of Vietnam broadband seismograph array data

Ling Bai [a,*], Takashi Iidaka [a], Hitoshi Kawakatsu [a], Yuichi Morita [a], N.Q. Dzung [b]

[a] Earthquake Research Institute, University of Tokyo, 1-1-1 Yayoi, Bunkyo-ku, Tokyo 113-0032, Japan
[b] Institute of Geophysics, Vietnam Academy of Science and Technology, 18 Hoang Quoc Viet Street, Quan Cau Giay, Hanoi 10000, Viet Nam

ARTICLE INFO

Article history:
Received 28 March 2008
Received in revised form 15 January 2009
Accepted 13 March 2009

Keywords:
Vietnam
Indochina block
Mantle flow
Seismic anisotropy
Shear-wave splitting

ABSTRACT

The Indochina block is located at the junction of four major plates. It has a close relationship with the uplift of Tibet plateau and the sea-floor spreading of the South China Sea in the geological evolution histories. We deployed a temporary broadband seismograph array in Vietnam from February 2000 to October 2005, and measured shear-wave splitting of core-refracted phases to investigate the upper mantle anisotropy beneath the Indochina block and adjacent regions. The observed delay times of up to 1.5 s are large, indicating a mantle source for the anisotropy. Two distinct regimes of seismic anisotropy are revealed. The fast polarization directions in the northern Indochina block with a main trend of N100°E are almost consistent with the direction of both the surface displacement and the absolute plate motion. These observations suggest the anisotropy is possibly generated by the present-day asthenospheric flow caused by the India–Eurasia collision. The fast polarization directions in the southern Indochina block and the Hainan island are nearly N60°E. The anisotropy in this area may reflect a combination of the India–Eurasia collision and the past orogenies in the lithosphere, or an abrupt variation in the asthenospheric flow.

1. Introduction

The Indochina block and adjacent regions (rectangle in Fig. 1(a)) are located at the junction of four major plates, which are India, Eurasia, Philippine Sea, and Pacific plates. This region is traversed by several major strike-slip faults that are easily recognizable on satellite image (Huchon et al., 1994). The Indochina block is separated from the south China block by the Red River fault at northeast, and from the Burma block by the Sagaing fault at northwest (Bird, 2003)(Fig. 1(b)). The south China block is classically separated into the Yangtze craton to the northwest and the southeast China orogenic belt to southeast (Charvet et al., 1996). The India–Eurasia collision started at about 55 Ma and controlled the Cenozoic tectonic history of southeast Asia (Tapponnier et al., 1982). The extrusion of the Indochina block southeastward is caused by the India–Eurasia collision and the accommodation of the opening of South China Sea (Molnar and Tapponnier, 1975; Briais et al., 1993).

Several studies have been performed to explain the tectonic activities of the Indochina block and adjacent regions. Previous shear-wave splitting studies (Luo et al., 2004; Flesch et al., 2005; Lev et al., 2006; Huang et al., 2007; Sol et al., 2007) based on limited IRIS data have shown that the seismic anisotropy beneath the Indochina block is larger than that beneath southwestern China where substantial crustal/mantle deformation took place in association with the India–Eurasia continental collision. Tomographic studies (e.g., Fukao et al., 2001; Lebedev and Nolet, 2003) have revealed prominent low velocity anomalies at 150 km depth and deeper beneath southern Indochina block, Hainan island, and southern part of the southeast China orogenic belt in association with a deep-mantle plume (Tu et al., 1991; Montelli et al., 2006). However, the detailed structure and physical properties of the Earth's interior beneath the Indochina block are largely unknown because of the lack of seismic observations.

Because seismic anisotropy provides information on the mantle flow (Nicolas and Christensen, 1987; Mainprice et al., 2000), it would be of a great importance to constrain the tectonic and geodynamic processes in the Earth. Such anisotropy can be probed using a variety of seismological tools, including shear-wave splitting (Vinnik et al., 1989), anisotropic receiver function (Levin and Park, 1998). The basic idea of shear-wave splitting has been widely applied for continental and oceanic areas since the late 1970s (Kosarev et al., 1979).

In order to investigate the tectonic process beneath the Indochina block, we measure shear-wave splitting of core-refracted phases (SKS and SKKS) for 45 teleseismic events using data from the Vietnam broadband seismograph array which was deployed during a period between February 2000 and October 2005 (Morita, 2001;

* Corresponding author. Fax: +81 3 3812 9417.
E-mail address: bai@eri.u-tokyo.ac.jp (L. Bai).

0031-9201/$ – see front matter © 2009 Elsevier B.V. All rights reserved.
doi:10.1016/j.pepi.2009.03.008

Takeuchi et al., 2008) and from IRIS station KMI, QIZ, and CHTO. The splitting observations with new data provide a more detailed picture of seismic anisotropy in the upper mantle beneath southeast Asia. The splitting results and its interpretation are important to improve our understanding of how southeast China deformed in response to the India–Eurasia collision and the sea-floor spreading during the Late Mesozoic to Cenozoic.

2. Vietnam broadband seismograph array and data selection

We deployed the Vietnam broadband seismograph array during a period between February 2000 and October 2005 as a part of the Ocean Hemisphere network Project (OHP; http://www.eri-ndc.eri.u-tokyo.ac.jp/) (Morita, 2001; solid triangles in Fig. 1(b)).

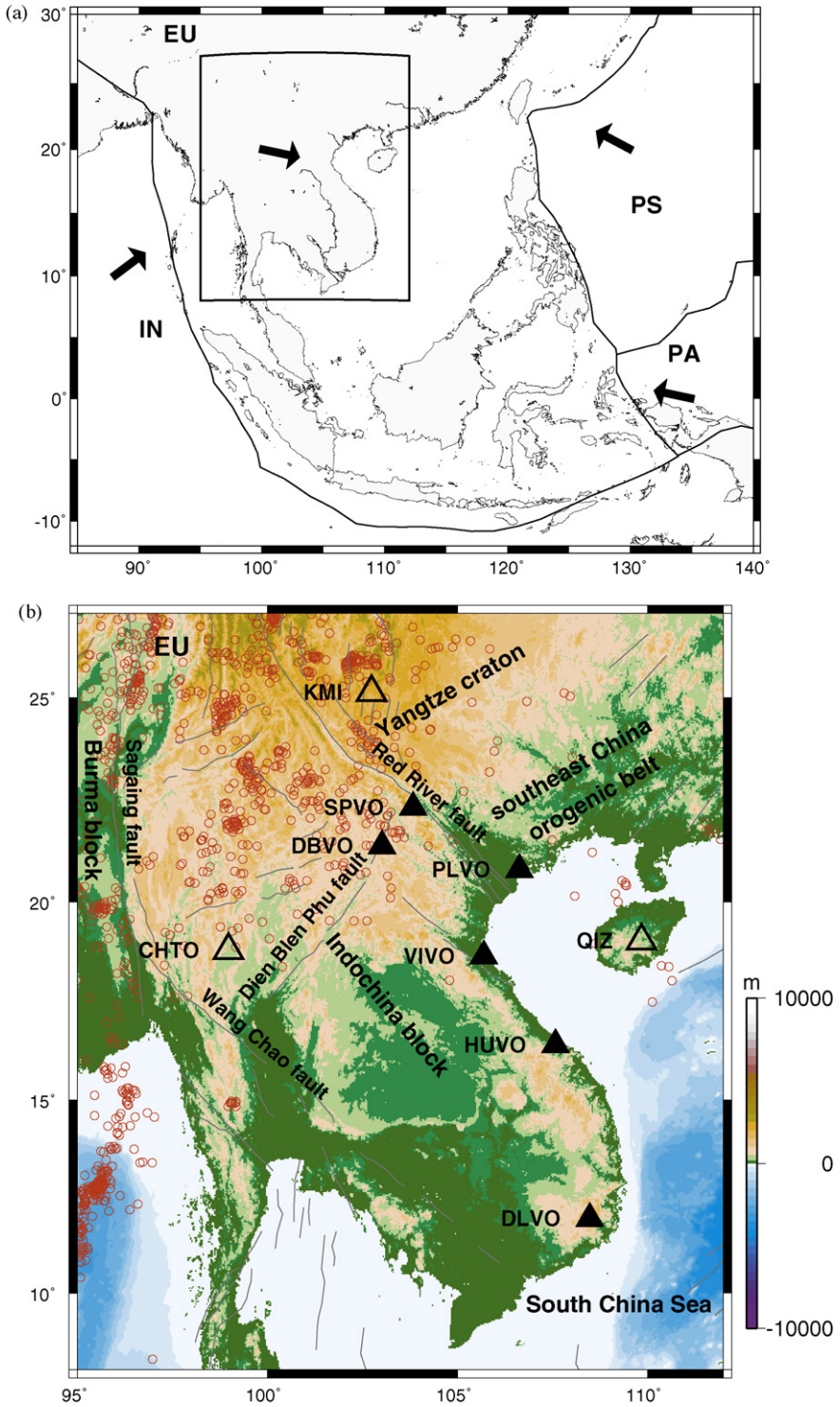

Fig. 1. (a) The study area (rectangle) located at the junction of four major plates, including India (IN), Eurasia (EU), Philippine Sea (PS), and Pacific (PA) plates. Thick lines indicate plate boundaries. Arrows show absolute plate movement of major plates (calculated at website http://www.sps.unavco.orgby using GSRM v1.2 model). (b) Locations of Vietnam array (solid triangles) and IRIS stations (open triangles) used in this study. Gray lines are active faults (Iwakuni et al., 2004). Red dots are earthquakes of $M \geq 3$ ($0 \leq$ depth ≤ 40 km) during the period of 1964/01/01–2005/12/31 taken from IRIS catalog. The background shows topography.

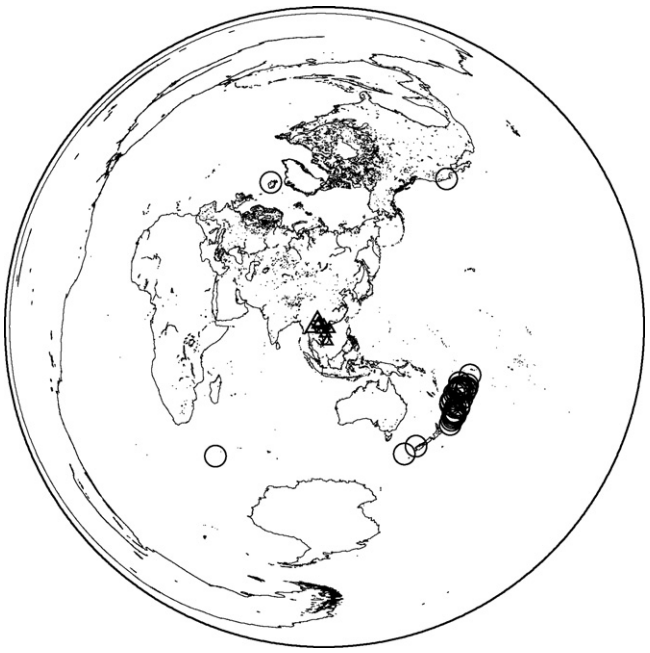

Fig. 2. 45 events that provide splitting parameters with small errors are used (open circles). Triangles show six seismic stations of the array and three IRIS stations.

This array consists of 6 broadband seismometers (Guralp CMG-3T) recorded at a sampling rate of 50 Hz. A compact hard disk drive was employed for data storage, which enables long-term and stable observation. The purpose of the deployment was to study deep structure of the Earth (e.g., Takeuchi et al., 2008), as well as to study the regional structure in and around Vietnam.

To investigate the seismic anisotropy in and around Vietnam region, we supplement the Vietnam array data with those recorded by three nearby permanent stations of IRIS between January 2000 and December 2005 (open triangles in Fig. 1(b)). We select clear recordings of teleseismic SKS and SKKS phases at epicentral distances of 80° to 120°. In the Advanced National Seismic System catalog (http://www.ncedc.org/cnss/catalog-search.html), there are about 650 earthquakes during the period between January 2000 and December 2005 with magnitudes equal to or greater than 5.5. Among the 650 events, 45 events provide data with high signal-to-noise ratio and splitting parameters with small errors. All the 45 events are shown in Fig. 2 and also listed in Table 1.

3. Shear-wave splitting analyses

Upon propagation through an anisotropic medium, a shear wave may split into fast and slow components. In order to determine the fast polarization direction (FPD, ϕ) and the delay time (δt) between the fast and slow components, we utilize a shear-wave splitting method of Silver and Chan (1991) as modified by Walker et al.

Table 1
Selected events.

ID	Data	Time	λ_E(°)	φ_N(°)	H (km)	M_W(Me)	Observation no.
00020005	2000/01/20	00:59:23.71	−176.5630	−28.2270	33.00	5.80	2
00089071	2000/03/29	07:13:53.01	−176.3090	−28.1270	10.00	5.80	1
00102064	2000/04/11	06:41:26.17	−178.3860	−27.9440	201.20	5.80	1
00109172	2000/04/18	17:28:12.39	−176.4690	−20.6640	220.70	(6.00)	2
00125203	2000/05/04	20:36:32.48	−178.5220	−17.9140	515.80	(6.50)	1
00166021	2000/06/14	02:15:25.84	178.0460	−25.5160	604.60	(6.40)	2
00173005	2000/06/21	00:51:46.88	−20.7580	63.9800	10.00	6.50	1
01139173	2001/05/19	17:36:25.59	−177.5150	−19.9030	368.70	6.00	1
01154024	2001/06/03	02:41:57.16	−178.6330	−29.6660	178.10	7.20	1
01269212	2001/09/26	21:31:12.23	178.1580	−26.5590	631.10	5.90	1
01334180	2001/11/30	18:02:06.30	−178.4820	−33.2480	10.00	5.70	2
02025032	2002/01/25	03:28:11.67	−178.7630	−20.8650	576.40	5.70	1
02181212	2002/06/30	21:29:36.30	179.2500	−22.2010	620.40	6.50	1
02231110	2002/08/19	11:01:01.19	−179.5130	−21.6960	580.00	7.70	1
02290042	2002/10/17	04:23:55.94	−178.4010	−19.8420	627.60	6.20	1
02295113	2002/10/22	11:39:04.21	−178.3910	−20.6330	549.00	6.20	1
03004051	2003/01/04	05:15:03.84	−177.6610	−20.5700	378.00	6.50	2
03124131	2003/05/04	13:15:18.66	−178.2320	−30.5310	62.40	6.70	1
03124200	2003/05/04	20:08:46.48	−178.2900	−30.5870	45.60	6.40	1
03129202	2003/05/09	20:26:15.98	32.2720	−48.2090	10.00	6.30	2
03139104	2003/05/19	10:43:22.68	−178.6700	−18.0440	563.80	6.00	1
03156082	2003/06/05	08:23:17.44	−178.8040	−30.6180	115.20	5.80	3
03184062	2003/07/03	06:21:50.37	−174.5220	−21.2780	10.00	6.00	1
03208020	2003/07/27	02:04:11.53	−176.5850	−21.0800	212.90	6.60	1
03226182	2003/08/14	18:23:06.26	−177.9840	−19.8990	563.30	5.90	1
03240203	2003/08/28	20:39:46.97	−179.5840	−21.9830	602.00	5.50	1
03273140	2003/09/30	14:08:37.74	−177.3980	−30.4370	10.00	6.40	2
03306053	2003/11/02	05:32:15.72	166.5350	−45.1900	10.00	6.40	1
03356191	2003/12/22	19:15:56.26	−121.0973	35.7002	8.05	6.50	2
03359141	2003/12/25	14:21:14.94	−178.2490	−34.9540	34.60	6.00	1
04057133	2004/02/26	13:35:16.19	−176.5400	−27.7810	10.00	5.60	2
04070034	2004/03/10	03:48:36.54	−178.1190	−32.3430	10.00	5.70	1
04094132	2004/04/03	13:29:32.29	−174.0600	−20.5350	2.20	5.80	1
04107165	2004/04/16	16:58:36.94	−175.8790	−24.5220	10.00	6.00	1
04143062	2004/05/22	06:28:08.31	−174.2160	−20.9010	10.00	5.50	1
04151211	2004/05/30	21:11:25.39	−177.1170	−31.0520	10.00	5.90	4
04166200	2004/06/14	20:06:13.29	−174.9370	−22.0870	10.00	5.80	1
04328210	2004/11/23	21:04:55.51	178.9900	−24.2940	532.30	5.90	1
04352071	2004/12/17	07:13:11.04	−179.3010	−21.9010	593.30	5.80	1
04358195	2004/12/23	19:50:05.09	161.4480	−49.3100	10.00	5.60	1
05022112	2005/01/22	11:27:43.16	−177.9290	−31.6100	23.50	5.70	1
05115023	2005/04/25	02:32:45.27	−176.5300	−27.0930	32.20	5.60	1
05124085	2005/05/04	08:57:01.05	−173.8290	−19.4070	22.80	5.90	1
05140124	2005/05/20	12:40:42.41	178.8400	−24.5290	565.30	6.00	1
05341233	2005/12/07	23:32:51.55	−177.6370	−30.0120	21.00	6.40	1

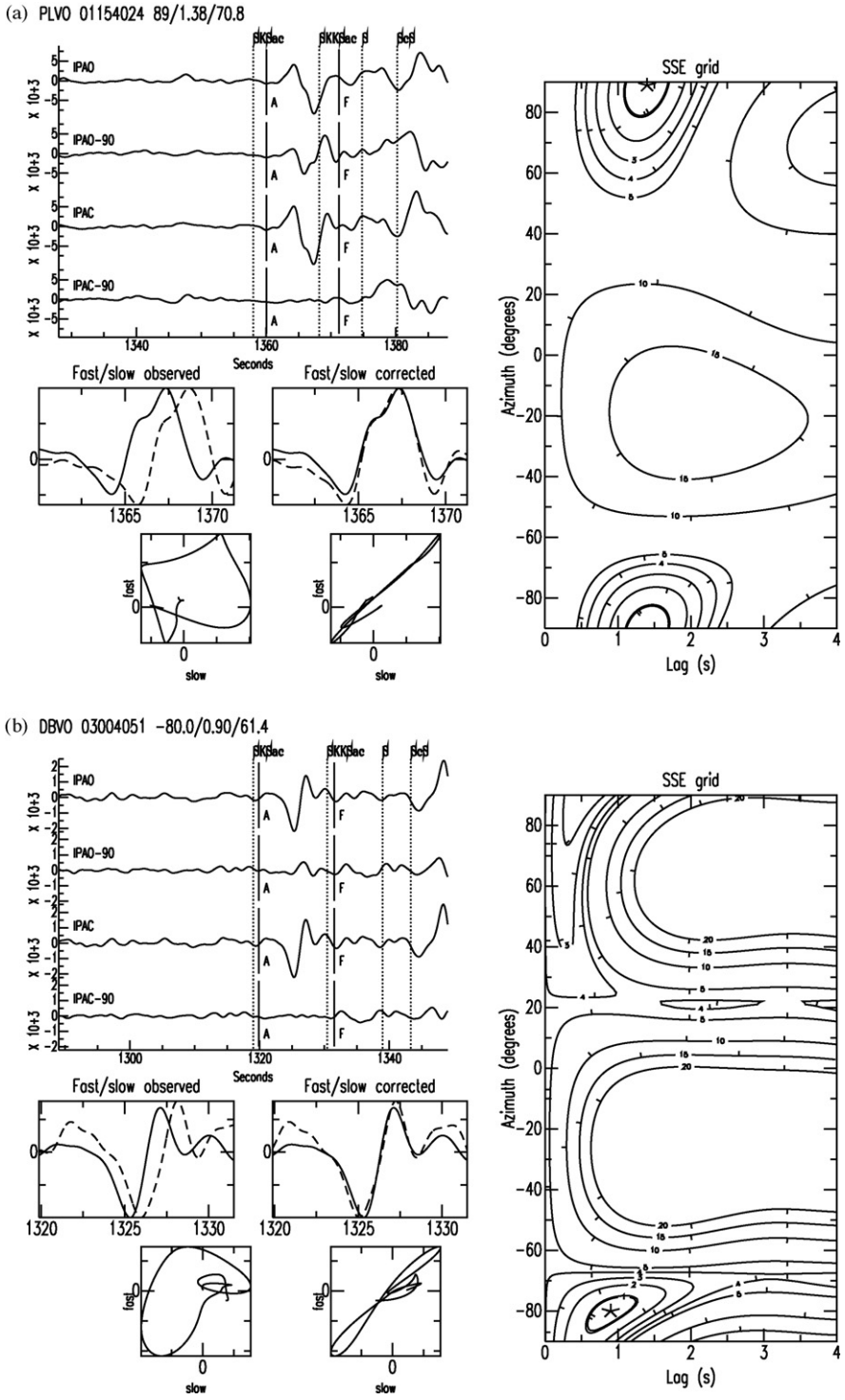

Fig. 3. Examples of shear-wave splitting analysis from stations (a) PLVO and (b) DBVO. Upper left: recorded radial, transverse component of the original waveforms (IPAO, IPAO-90°) and anisotropy-corrected waveforms (IPAC, IPAC-90°) (IPAO: observed incident polarization azimuth, IPAC: corrected incident polarization azimuth.). Dashed lines show IASP91 predicted phase arrival times. Vertical solid lines show picked time window between A and F on which splitting measurement is made. Lower left: fast (solid line) and slow (dashed line) waves and corresponding horizontal particle motion. Right: misfit grid shows the 95% confidence region (double contour) and the optimum ϕ and δt (asterisk). Titles indicate the station, event ID, and the optimum parameters with signal-to-noise ratio (ϕ/ δt/SNR), respectively.

(2004) for individual earthquakes. A grid search over possible values is performed to linearize the shear-wave particle motion when the effect of the anisotropy is removed. Fig. 3 gives examples of waveform splitting from two Vietnam array stations. All records are band-pass filtered between 0.02 and 1.0 Hz to reduce the background noise. The master time windows used are 10–15 s around the phases of interest based on the predicted travel times from the iasp91 model (Kennett and Engdahl, 1991).

The accuracy of resulting splitting parameters can be controlled by several factors, including (1) the signal-to-noise ratio (SNR) of the data, (2) the back azimuth separation from the fast or slow polarization directions (ΔBAZ), (3) the quality of the SKS arrivals. Synthetic analysis indicates that splitting is confidently detectable at SNR $>$ 8 regardless of the wave's original polarization orientation, and detectable at an SNR value of 4 with $|\Delta$ BAZ $|$ larger than 20° (Restivo and Helffrich, 1999). Studies on the comparison of dif-

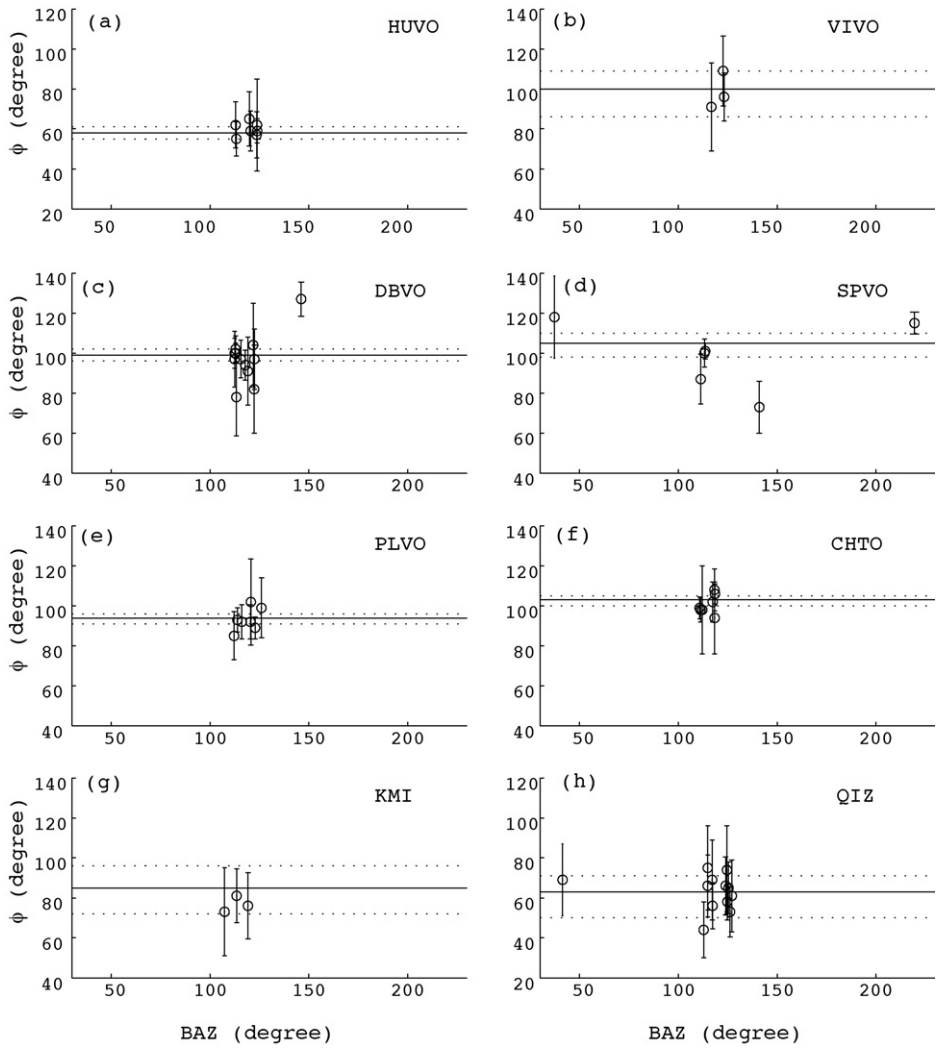

Fig. 4. Graphs with FPD versus BAZ. Open dots and vertical lines indicate FPDs and corresponding uncertainties. Horizontal real line and two dotted lines are the station FPD, $-2\,\sigma$ and $2\,\sigma$ uncertainties calculated from stacking the apparent splitting measurements. For simplicity, range is given as $0^\circ \leq\phi\leq 180^\circ$ rather than $-90^\circ \leq\phi\leq 90^\circ$.

ferent signal processing techniques (Long and van der Hilst, 2005; Wüstefeld and Bokelmann, 2007) show that the methodology of Silver and Chan (1991) is reliable for cases with $|\Delta$ BAZ $|$ down to 10 $^\circ$. Besides, splitting parameters with large errors are often observed for data even with high SNR. The 95% confidence region ($2\,\sigma_\phi$ for ϕ, and $2\,\sigma_{\delta t}$ for δt) is determined via a method that is affected by the frequency content of the data Silver and Chan (1991). The signal sometimes does not contain an adequate frequency bandwidth to calculate the error bars, perhaps due to the confusion of SKS arrivals with other phases (e.g., S or ScS), large earthquake source dimensions, and/or attenuation along the ray path.

Based on these studies, only good measurements, which satisfy the following conditions, are used in this study to constrain the final result: (1) SNR $\geq$4; we defined the SNR as

$$SNR = \frac{\max|a_{r(A,F)}|}{\max|a_{t(A-(F-A),A)}|}, \quad (1)$$

where max $|a_{r(A,F)}|$ is the maximum amplitude on the radial component of seismogram in the SKS time window between A and F (see upper left of Fig. 3), and max $|a_{t(A-(F-A),A)}|$ is the maximum amplitude on the transverse component of seismogram just prior to time A for a window length of $|F-A|$. (2) $2\sigma_\phi < 22.5^\circ$ and $2\sigma_{\delta t} < 1.0$ s. Our data all satisfy the condition, $|\Delta$ BAZ $| \geq 10^\circ$.

4. Splitting results

We measure a total of 58 apparent splitting parameters: including 49 from SKS phases and nine from SKKS phases. For station DLVO, the epicentral distances from most of the selected events are close to 80°. At these distances, the SKS phase is considered to be contaminated by other phases. The shear-wave splitting results obtained in this seismic station are thus not included in the results. Fig. 4 shows fast polarization directions (FPDs) with respect to back azimuths (BAZs) for other five Vietnam array stations and three IRIS stations. For most stations, the measurements of FPD yield consistent values. However, the majority of the events used lie in Tonga and adjacent regions. These events provide a limited azimuthal coverage. For a two-layer model, the splitting parameters are expected to depend strongly on the initial polarization of the waves (Silver and Savage, 1994). There is only one case in which a suggestion of azimuthal dependence of the splitting may be seen; for SPVO (Fig. 4(d)), the BAZs of several measurements range about 200°. The 95% confidence regions for two subsets at 140° and 220° back azimuths lie outside the confidence region for all of the measurements. However, a greater sampling of splitting measurements and BAZ range will be required to detect complex upper mantle structure. We further consider the presence of such a two-layer model

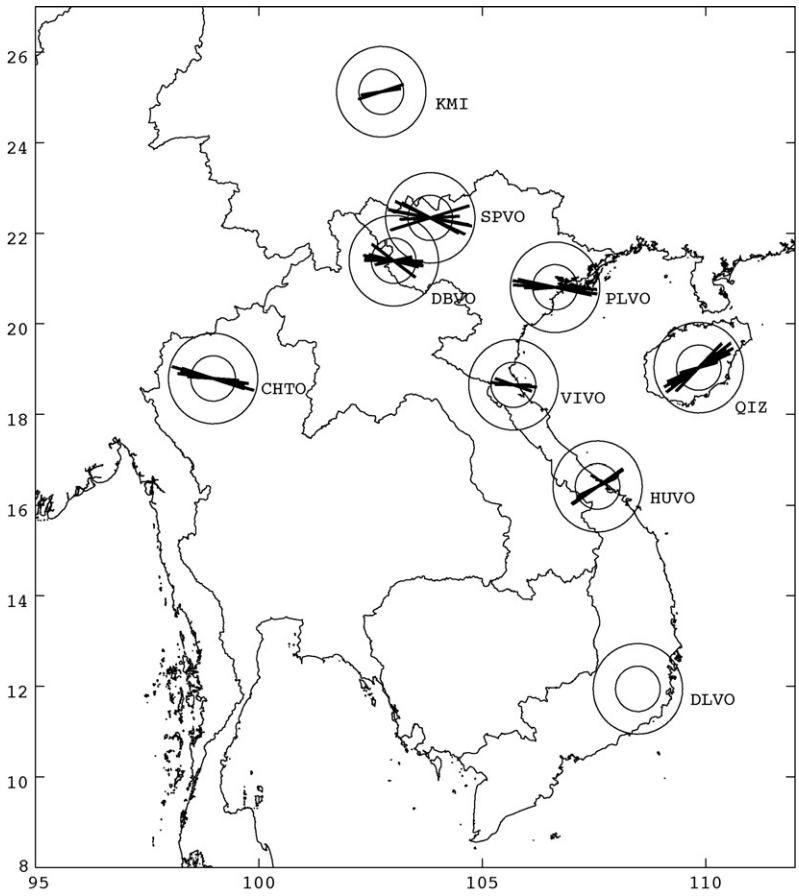

Fig. 5. The obtained results of shear-wave splitting. The orientation and length of each bar indicate FPD and delay time, respectively. The concentric circles represent the delay times of 1 s and 2 s. Circles without bars indicate unconstrained measurement.

under the assumption of one layer in Section 5.3. The splitting parameters of individual records are shown in Fig. 5 and listed in Table 2.

After these individual event splitting parameter measurements, the splitting parameter for each station is derived by stacking. We use a multi-event stacking procedure of Wolfe and Silver (1998) to stack the error surface of individual earthquakes and reduce the uncertainty on the estimation of ϕ and δt at each station. The result of final station splitting parameters are presented in Fig. 6 and Table 3.

The splitting results fall into three groups (Fig. 5): (1) in south China block (KMI): the average FPD is N85°E with an average delay time of 0.74 s; (2) in northern Indochina block (SPVO, DBVO, PLVO, CHTO and VIVO): the average FPD is N100°E with an average delay time of 1.13 s; (3) in southern Indochina block (HUVO) and Hainan island (QIZ): the average FPD is N61°E with an average delay time of 1.01 s.

Fig. 7 shows the comparison of shear-wave splitting analyses with other studies, which are shown with green bars. Luo et al. (2004) and Zhao et al. (2007) made measurements of SKS wave splitting for three IRIS stations using the methodology of Silver and Chan (1991) and data from 1990 to 2003, and from 2000 to 2004, respectively. Their observations (exception for Zhao et al., 2007 at KMI) are consistent with our results. Lev et al. (2006) employed a temporary array of 25 IRIS-PASSCAL stations at southwest China around KMI, both the FPD and delay time at KMI is in good agreement with ours. Huang et al. (2007) set up a broadband seismic array across the northwestern Red River fault zone, most stations in northern Indochina block showed consistent splitting parameters with us. In addition, Flesch et al. (2005) and Sol et al. (2007) estimated splitting measurements for some stations in our study area.

5. Discussion

5.1. Source of the anisotropic signal

As the ray path of core-refracted waves is nearly vertical through the mantle and crust, the estimated anisotropy is located within nearly vertical volume beneath the station and thus difficult to determine the source depth. The petrophysics analysis has quantified the amplitude of the delay times that could be expected in the crust (Barruol and Mainprice, 1993). Mainprice et al. (2005) have shown that seismic anisotropy likely lies in the uppermost 300 km of the Earth and Sieminski et al. (2007) has shown that SKS is likely mostly sensitive to anisotropy in the uppermost 400 km of the Earth. Silver (1996) studied contributions of various layers in the Earth to SKS splitting times. He found the average contribution from the crust to be 0.2 s, and the contribution from the lower mantle and transition zone to be typically less than 0.2 s. Hall et al. (2004) commented the effect of lower-mantle anisotropy on SKS and SKKS phases to be less than 0.5 s. Thomas et al. (2007) showed evidence for radial anisotropy (transverse isotropy with a radial symmetry axis) in the lowermost mantle beneath Southeast Asia, which affect little on the SKS splitting. With the Moho depths of 30–45 km (Lebedev and Nolet, 2003; Mooney et al., 1998), the crustal contribution in the Indochina block may be close to the average value of 0.2 s. The observed values of delay times for the Indochina block range between 0.84 and 1.46 s, which is generally considered too large to be of crustal origin. By contrast with the

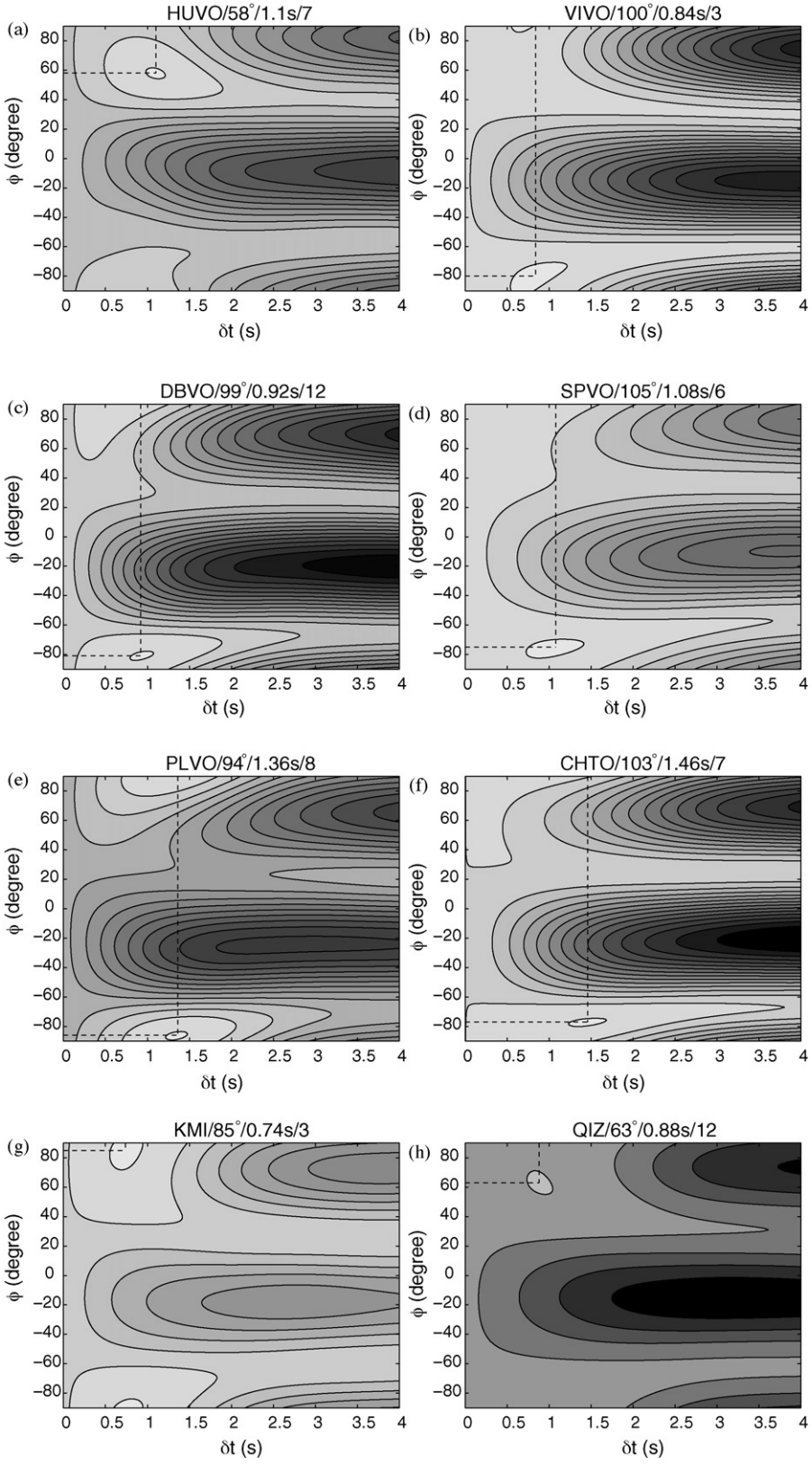

Fig. 6. The shear-wave splitting results derived by stacking procedure at each station. The optimum splitting parameters are shown by crosses of broken lines, and the 95% confidence region are indicated in the lightest ranges. The title gives the station name, FPD, delay time, and number of events analyzed in order.

south China block (KMI) that has smaller delay time of 0.74 s and larger crustal thickness of 50–70 km, the contribution from upper mantle anisotropy appears much larger beneath the Indochina block.

One of the most important anisotropic minerals is olivine, which comprises much of the upper mantle. An average maximum shear-wave anisotropy for the olivine component in real rocks has been suggested to be 9% (Mainprice and Silver, 1993). At global scale,

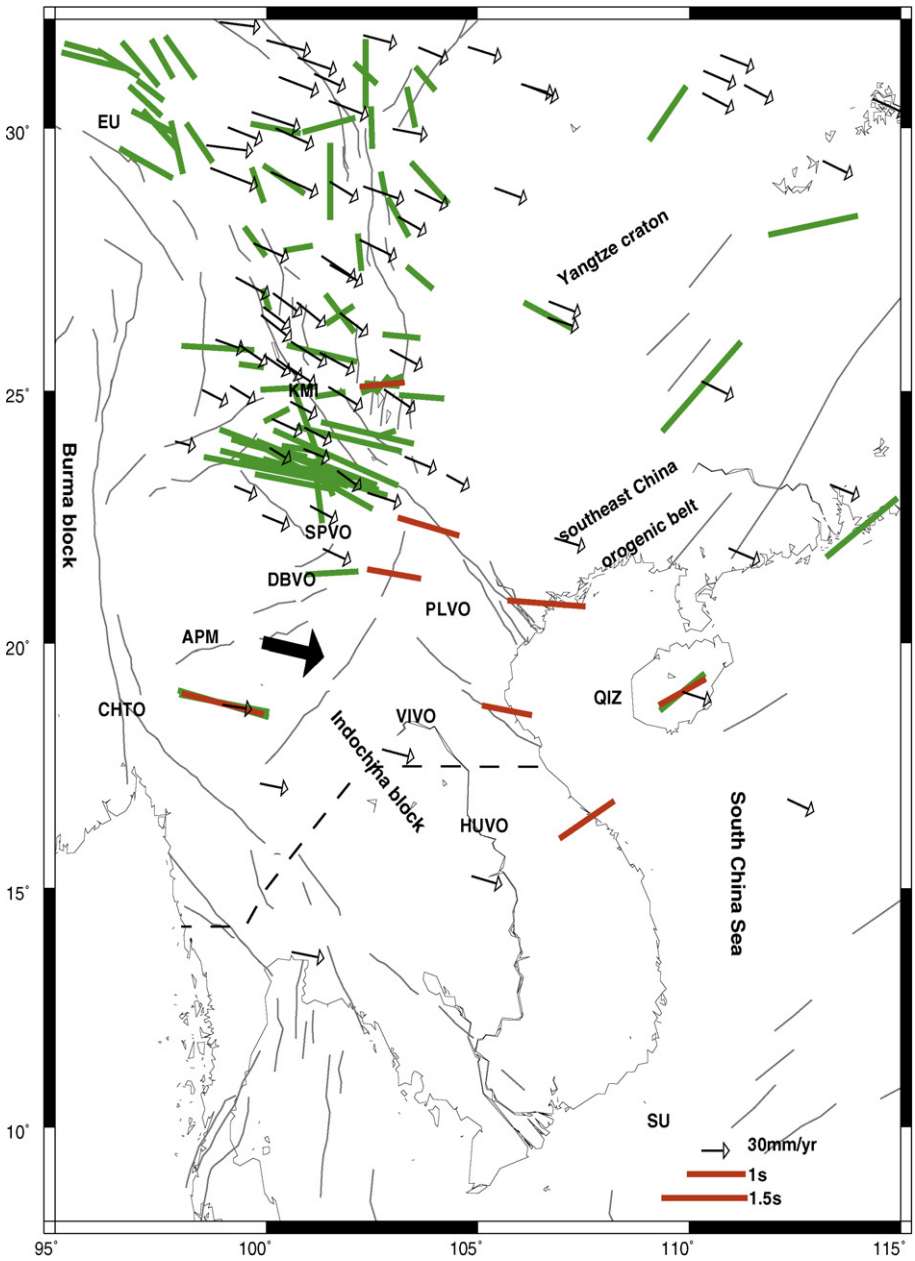

Fig. 7. Comparison of shear-wave splitting with other studies. Red bars are splitting from this study. Green bars are from other studies (Luo et al., 2004; Flesch et al., 2005; Lev et al., 2006; Huang et al., 2007; Sol et al., 2007; Zhao et al., 2007). Thin arrows indicate GPS station velocities on the ITRF no-net-rotation reference frame (data of Thailand are from Iwakuni et al., 2004, and others are from Wang et al., 2001). Thick arrow indicates average absolute plate motion direction of the Eurasia plate by taking into account several plate motion models. Dashed line shows the estimated inland boundary between the Eurasia plate and Sunda plate (SU) (Bird, 2003). Other symbols are the same as Fig. 1(b).

3–10% of anisotropy has been found in the upper mantle (e.g., Nataf et al., 1984). Assuming a mean shear-wave velocity of about 4.6 km/s with 5% anisotropy, our observed delay times of 0.84–1.46 s roughly correspond to thicknesses of 80 to 135 km for the anisotropic layer.

5.2. The influence of the India–Eurasia collision on northern Indochina block

The India–Eurasia collision started at about 55 Ma and controlled the Cenozoic tectonic history of southeastern Asia (Tapponnier et al., 1982). Between 50 and 23 Ma, the eastern syntaxis of India moved from lat 10°N to lat 20°N. Indochina was in the domain of active extrusion at that time (Huchon et al., 1994). Both geological (Wang et al., 1998) and geodetic (King et al., 1997; Chen et al., 2000; Wang et al., 2001) evidences show that the region of eastern Tibet plateau currently rotates with a velocity of about 6 mm/year relative to the south China block. This rotation creates a left lateral shear in northern Indochina block.

Our observed FPDs vary throughout the study area and are therefore not explained by a simple hypothesis. However, absolute plate motion (APM) determined for the Indochina block trends N105°E ±5° in several plate motion models (calculated at website http://www.sps.unavco.org). The FPDs in northern Indochina block are approximately parallel to the APM. It argues for a simple asthenospheric flow model for the cause of observed anisotropy (e.g., Silver and Chan, 1991; Vinnik et al., 1992). These versions of the asthenospheric flow hypothesis assume that the anisotropy is due to the passive shearing in the asthenosphere by the moving

Table 2
Summary of the SKS and SKKS measurements.

Station	Event ID	ϕ(°)	2 σ_ϕ(°)	δt(s)	2 $\sigma_{\delta t}$(s)	Phase
HUVO	03124131	57	11.5	1.36	0.52	SKKS
	03156082	59	6.0	1.02	0.29	SKS
	04057133	59	10.0	1.08	0.30	SKKS
	04094132	62	11.5	1.04	0.29	SKKS
	04143062	55	8.5	1.38	0.24	SKS
	04151211	62	22.0	0.88	0.61	SKS
	05115023	65	13.5	0.92	0.29	SKKS
VIVO	03273140	−71	17.5	0.86	0.98	SKS
	04107165	−89	22.0	0.82	0.53	SKS
	04151211	−84	12.0	1.04	0.34	SKS
DBVO	02181212	−83	9.5	1.30	0.48	SKS
	03004051	−80	5.0	0.90	0.32	SKS
	03156082	−83	15.0	0.92	0.68	SKS
	03184062	−83	14.0	1.08	0.82	SKS
	03208020	−78	6.5	1.08	0.50	SKS
	03226182	−80	7.5	1.34	0.62	SKS
	03273140	−76	21.0	1.14	0.96	SKS
	04057133	−89	17.0	1.32	0.53	SKS
	04151211	82	22.0	0.70	0.29	SKS
	04166200	78	19.5	0.84	0.42	SKKS
	04358195	−53	8.5	1.22	0.46	SKS
	05140124	−86	7.5	1.20	0.29	SKS
SPVO	02295113	−79	4.0	1.90	0.48	SKS
	03004051	−80	7.0	1.76	0.65	SKS
	03129202	−65	5.5	1.72	0.63	SKS
	03139104	87	12.5	1.32	0.44	SKS
	03306053	73	13.0	1.82	0.88	SKKS
	03356191	−62	20.5	1.44	0.90	SKS
PLVO	00089071	−78	21.5	1.68	0.98	SKS
	00109172	−87	6.0	1.14	0.27	SKS
	00125203	85	12.0	0.96	0.37	SKS
	00166021	−88	8.5	1.40	0.31	SKS
	00173005	−87	18.0	1.80	0.51	SKS
	01154024	89	5.5	1.38	0.19	SKS
	01334080	−81	15.0	1.90	0.50	SKS
	02231110	−88	8.5	1.42	0.45	SKS
CHTO	00020005	−72	10.5	1.52	0.99	SKS
	00102064	−74	5.0	1.90	0.42	SKS
	00109172	−82	6.0	1.60	0.46	SKS
	00166021	−78	10.0	1.44	0.67	SKS
	01139173	−81	5.5	1.30	0.44	SKS
	01269212	−86	18.0	1.16	0.64	SKS
	02025032	−82	22.0	1.02	0.77	SKS
KMI	00020005	76	16.5	1.10	0.36	SKS
	03359141	81	13.5	0.88	0.28	SKKS
	04328210	73	22.0	0.36	0.84	SKS
QIZ	01334180	61	18.0	1.76	0.83	SKS
	02290042	75	21.0	0.76	0.29	SKKS
	03124200	66	15.5	1.50	0.42	SKKS
	03156082	58	9.0	1.46	0.44	SKS
	03240203	56	11.5	1.08	0.41	SKS
	03356191	69	18.0	0.78	0.38	SKS
	04070034	53	12.5	1.80	0.95	SKS
	04151211	74	22.0	0.90	0.58	SKS
	04352071	69	20.0	0.90	0.31	SKS
	05022112	65	13.0	1.46	0.49	SKS
	05124085	44	14.0	1.46	0.48	SKS
	05341233	66	14.5	1.54	0.58	SKS

plate. In addition, the crustal movements observed by GPS measurements in Thailand (Iwakuni et al., 2004) are also parallel to the FPDs. Based on these observations, we may infer that the crust and the upper mantle are coupled and the anisotropy beneath northern Indochina block was possibly generated by asthenospheric flow caused by India–Eurasia collision.

Two stations (SPVO and PLVO) of the Vietnam array are located directly on the Red River fault zone, which is a major tectonic feature in our study area. The FPDs are different between northeast (in the southeast China orogenic belt) and southwest sides of the

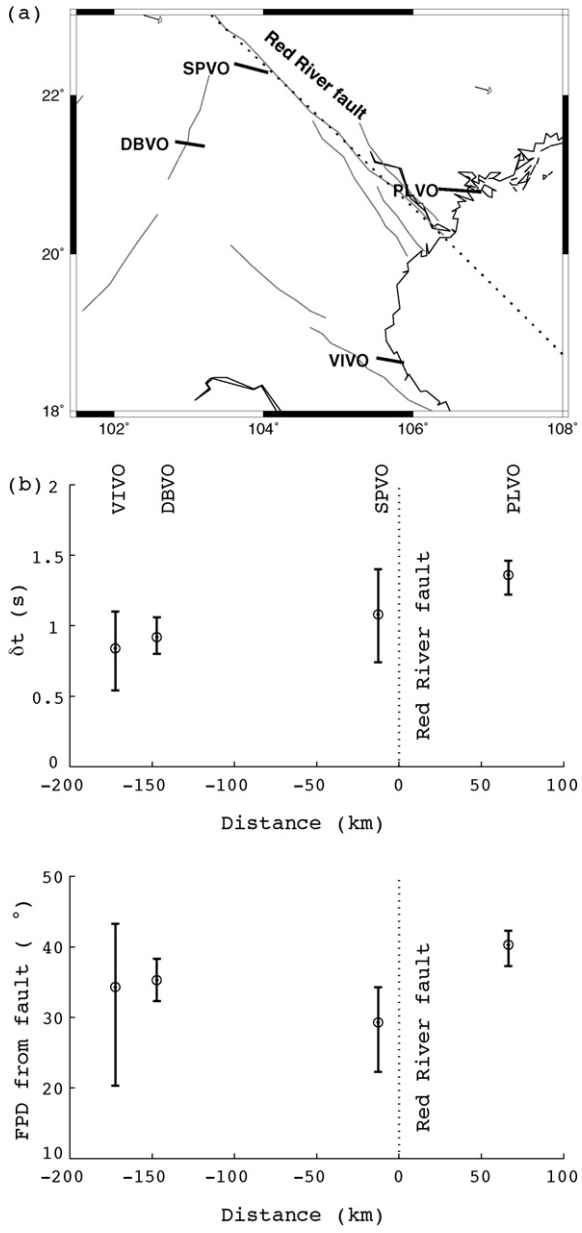

Fig. 8. (a) Zoom in on the Red River fault zone. Broken line shows average trend of the fault. (b) Delay time (upper plot) and FPD rotation angle from fault (lower plot) as a function of the fault-normal distance.

Red River fault. Although this observation itself supports the idea that the Red River fault plays a role of a major block boundary, the newly observed FPDs of the stations on the Red River fault (SPVO and PLVO) do not show apparent difference from those of stations away from the fault. However a careful examination of FPDs shows the effect of the fault. Fig. 8 shows variations in delay time (upper plot in Fig. 8(b)) and FPD rotation angle from the fault (lower plot in Fig. 8(b)) as a function of fault-normal distance. While the delay times increase from about 0.9 s (for VIVO and DBVO) to about 1.3 s (for SPVO and PLVO) with decreasing distance for the near-fault area, the rotation angles are nearly constant with an angle of about 35 degrees. The transpression model of Sanderson and Marchini (1984) predicts that the direction of the maximum finite-strain can be rotated by 10–40° from the main shear direction depending on the ratio of the compression and shear strain, and this affects in the same way for both sides of the fault. So the left-lateral motion along the Red River fault that ended at 23 Ma (Huchon et al., 1994) could

Table 3
Stations of Vietnam array (No. 1 to No. 6) and IRIS (No. 7 to No. 9) used for shear wave splitting analysis and their final results.

No.	Station	λ_E(°)	φ_N(°)	H (km)	ϕ(°)	$-2\sigma_\phi$(°)	$2\sigma_\phi$(°)	δt(s)	$-2\sigma_{\delta t}$(s)	$2\sigma_{\delta t}$(s)	n
1	HUVO	107.5800	16.4111	0.0260	58	−3	3	1.10	−0.10	0.10	7
2	VIVO	105.6964	18.6503	0.0160	−80	−14	9	0.84	−0.30	0.26	3
3	DBVO	103.0184	21.3905	0.5000	−81	−3	3	0.92	−0.12	0.14	12
4	SPVO	103.8353	22.3383	1.5850	−75	−7	5	1.08	−0.34	0.32	6
5	PLVO	106.6277	20.8050	0.0250	−86	−3	2	1.36	−0.14	0.10	8
6	DLVO	108.4817	11.9450	1.6010	–	–	–	–	–	–	–
7	CHTO	98.9769	18.7900	0.3160	−77	−3	2	1.46	−0.22	0.22	7
8	KMI	102.7400	25.1233	1.9400	85	−13	11	0.74	−0.18	0.20	3
9	QIZ	109.8433	19.0294	0.2300	63	−13	8	0.88	−0.14	0.16	12

The λ_E, φ_N, and H are longitude, latitude, and altitude of stations, respectively. ϕ and δt are the fast polarization direction and delay time with 2σ error bars. Mark – indicates unconstrained measurement, and n is the stacked number of records for each station.

enhance the signal of the seismic anisotropy due to asthenospheric flow which also shares a similar general direction. We, therefore, suggest that the 0.9 s delay might be due to the asthenosphere and the additional delay time of 0.4 s might be caused by the fault effect in the lithosphere.

5.3. Shearing strain in southern Indochina block and Hainan island

The FPDs in southern Indochina block (HUVO) and Hainan island (QIZ) are particularly interesting, as the FPDs are oriented northeast, in contrast with the APM that directs toward southeast. The difference of the directions of FPDs and APM prevents a simple explanation for the observed anisotropy. The source of mantle anisotropy in this area could be related to some local tectonic regime. Two models may explain the significant shift of the FPDs: (1) thickening of the lithosphere towards the South China Sea; or (2) abrupt variation of the asthenospheric flow under the study area.

In the southeast China orogenic belt (northeast of the Red River fault, southeast of the Yantze craton in Fig. 1(b)), observations from other studies show similar FPDs and delay times with those in Hainan and southern Indochina block (Fig. 7). Although the geodynamic regime is in debate (Li and Li, 2007), it is unambiguous that the southeast China orogenic belt and South China Sea contain widely northeast trending left-lateral strike-slip faults with ages of Late Mesozoic to Cenozoic (Li, 2000). It argues for vertically coherent deformation model in which the FPD is parallel to the orientation of surface faults (i.e., vertical shear planes) (Silver, 1996). The correlation between the FPDs and fault lineations may be regarded as a piece of evidence for the observed shear-wave splitting results being from anisotropy frozen within the lithosphere due to the left-lateral shear of the Late Mesozoic to Cenozoic (Li, 2000). This appears to support the model (1) such that under land the splitting would be controlled by the asthenosphere but offshore it would be a combination of asthenosphere and lithosphere. In order to illustrate the effect of two anisotropic layers, we apply the method of Silver and Savage (1994) on the southern Indochina block and Hainan island. Taking the asthenosphere (ϕ=105°, δt=0.9 s; an average of VIVO and DBVO as in the previous paragraph) as layer one, and the averaged apparent splitting parameters of station HUVO and QIZ (60.5°, 0.99 s) as the final result, then the splitting parameters of layer two within the lithosphere are found to be (48°, 0.7 s). This estimated FPD of the layer two is consistent with the shearing direction of the surface faults in the southeast China orogenic belt.

Tomographic studies have revealed prominent low velocity anomalies at 150 km depth and deeper beneath the southern Indochina block, the Hainan island and southern part of the southeast China orogenic belt (Fukao et al., 2001; Lebedev and Nolet, 2003). The Cenozoic basalts in these areas, particularly in Hainan, display the eruption morphology of the hot spot type volcanism, which is usually associated with deep-mantle plumes (Tu et al., 1991; Montelli et al., 2006). Large scale Cenozoic magmatic activities have been reported in these regions based on the $^{40}Ar/^{39}Ar$ dating result of Neogene basalts (Lee et al., 1998). These magmatic activities are estimated to be triggered by large amount of melts after the sea-floor spreading stopped at 16 Ma in the South China Sea (Lee et al., 1998). We therefore cannot deny a possibility that the mantle beneath the southern Indochina block, Hainan island and southern part of the southeast China orogenic belt are less viscous than adjacent regions and thus easier to generate a shearing strain. This hypothesis favors the model (2) and further studies are obviously needed to substantiate this speculation.

Recent studies have suggested the existence of a minor Sunda plate based on the observations of relative movements of south China and southeastern Asia with respect to the Eurasia plate (Chamot-Rooke and Le Pichon, 1999; Rangin et al., 1999). A northern inland boundary between the Eurasia plate and the postulated Sunda plate has been estimated to be at central Indochina block (Bird, 2003)(see the dashed black line in Fig. 7). This boundary is guided by the northern extent of the aseismic region and of smooth topography. It seems that the Indochina block is seismically active and deformed along with the Tibet plateau in the north, but behaves differently along with the South China Sea in the south.

6. Conclusions

We have investigated the upper mantle anisotropy beneath the Indochina block and adjacent regions at a temporary Vietnam array stations and IRIS stations. We observed the ubiquitous anisotropic structure beneath the stations. The primary source of observed anisotropy is located in the upper mantle. The FPDs in northern Indochina block are almost parallel to the surface displacement and the APM, indicating that the crust and upper mantle are coupled and the anisotropy is possibly generated by the asthenospheric flow caused by India–Eurasia collision. The FPDs in southern Indochina block and Hainan island show different directions from the APM. The anisotropy in this area may reflect a combination of signals from the asthenosphere and the lithosphere, or an abrupt variation in the asthenospheric flow.

Acknowledgements

We are grateful to Paul Silver and Kris Walker for the use of their shear-wave splitting codes. We thank Jean-Paul Montagner for giving comments on the early version of the manuscript, Lucy Flesch for useful discussion on modeling of mantle flow, and Michael Kendall and James Wookey for giving advice on the presence of two anisotropic layers. Constructive comments are due to Guilhem Barruol, an anonymous reviewer, and editor George Helffrich. The topographic data are extracted from the National Geophysical Data Center. Some waveforms are provided by the IRIS Data Management Center. GMT was used for making some of the figures. This study

was funded by a Research Fellowship of the Japan Society for the Promotion of Science (JSPS).

References

Bird, P., 2003. An updated digital model of plate boundaries. Geochem. Geophys. Geosyst. 4, 1027, doi:10.1029/2001GC000252.

Barruol, G., Mainprice, D., 1993. A quantitative evaluation of the contribution of crustal rocks to the shear wave splitting of teleseismic SKS waves. Phys. Earth Planet. Int. 78, 281–300, doi:10.1016/0031-9201(93)90161-2.

Briais, A., Patriat, P., Tapponier, P., 1993. Updated interpretation of magnetic anomalies and seafloor spreading stages in the South China Sea: Implications for the Tertiary tectonics of Southeast Asia. J. Geophys. Res. 98, 6299–6328.

Chamot-Rooke, N., Le Pichon, X., 1999. GPS determined eastward Sundaland motion with respect to Eurasia confirmed by earthquakes slip vectors at Sunda and Philippine trenches. Earth Planet. Sci. Lett. 173, 439–455.

Charvet, J., Shu, L.S., Shi, Y.S., Guo, L.Z., Faure, M., 1996. The building of south China: collision of Yangzi and Cathaysia blocks, problems and tentative answers. J. Southeast Asian Sci. 13, 223–235.

Chen, Z., Burchfiel, B.C., Liu, Y., King, R.W., Royden, L.H., Tang, W., Wang, E., Zhao, J., Zhang, X., 2000. Global Positioning System measurements from eastern Tibet and their implications for India/Eurasia intercontinental deformation. J. Geophys. Res. 105, 16215–16227.

Flesch, L.M., Holt, W.E., Silver, P.G., Stephenson, M., Wang, C.Y., Chan, W.W., 2005. Constraining the extent of crust-mantle coupling in central Asia using GPS, geologic and shear wave splitting data. Earth Planet. Sci. Lett. 238, 248–268.

Fukao, Y., Widiyantoro, S., Obayashi, M., 2001. Stagnant slabs in the upper and lower mantle transition region. Rev. Geophys. 39, 291–323.

Hall, S.A., Kendall, J.M., Van der Baan, M., 2004. Some comments on the effects of lower-mantle anisotropy on SKS and SKKS phases. Phys. Earth Planet. Int. 146, 469–481.

Huang, Z., Wang, L., Xu, M., Liu, J., Mi, N., Liu, S., 2007. Shear wave splitting across the Ailao Shan-red River fault zone, SW China. Geophys. Res. Lett. 34, doi:10.1029/2007GL031236.

Huchon, P., Le Pichon, X., Rangin, C., 1994. Indochina peninsula and the collision of India and Eurasia. Geology 22, 27–30.

Iwakuni, M., Kato, T., Takiguchi, H., Nakaegawa, T., Satomura, M., 2004. Crustal deformation in Thailand and tectonics of Indochina peninsula as seen from GPS observations. Geophys. Res. Lett. 31, L11612, doi:10.1029/2004GL020347.

Kennett, B.L.N., Engdahl, E.R., 1991. Travel times for global earthquake location and phase identification. Geophys. J. Int. 105, 429–465.

King, R.W., Shen, F., Burchfiel, B.C., Royden, L.H., Wang, E., Chen, Z., Liu, Y., Zhang, X., Zhao, J., Li, Y., 1997. Geodetic measurement of crustal motion in southwest China. Geology 25, 179–182.

Kosarev, G.L., Makeyeva, L.I., Savarensky, Ye.F., Chesnolov, Ye.M., 1979. Influence of anisotropy under a seismograph station on the records of body waves. Izvestiya, Phys. Solid Earth 15, 102–110.

Lebedev, S., Nolet, G., 2003. Upper mantle beneath Southeast Asia from S velocity tomography. J. Geophys. Res. 108, 2048–2074.

Lee, T.Y., Lo, C.H., Chung, S.L., Chen, C.Y., Wang, P.L., Lin, W.P., Hoang, N., Chi, C.T., Yem, N.T., 1998. $^{40}Ar/^{39}Ar$ dating result of Neogene basalts in Vietnam and its tectonic implication,. In: Flower, M.F.J., Chung, S.L., Lo, C.H., Lee, T.Y. (Eds.), Mantle Dynamics and Plate Interactions in East Asia, vol. 27. AGU, Geodynamics Ser, Washington D.C, pp. 317–330.

Lev, E., Long, M.D., van der Hilst, R.D., 2006. Seismic anisotropy in Eastern Tibet from shear wave splitting reveals changes in lithospheric deformation. Earth. Planet. Sci. Lett. 251, 293–304.

Levin, V., Park, J., 1998. P-SH conversions in layered media with hexagonally symmetric anisotropy: a cookbook. Pure Appl. Geophys. 141, 669–697.

Li, X.H., 2000. Cretaceous magmatism and lithospheric extension in Southeast China. J. Southeast Asian Sci. 18, 293–305.

Li, Z.X., Li, X.H., 2007. Formation of the 1300-km-wide intracontinental orogen and postorogenic magmatic province in Mesozoic South China: A flat-slab subduction model, Geology 35, 179–182, doi:10.1130/G23193A.1.

Long, M.D., van der Hilst, R.D., 2005. Estimating shear-Wave splitting parameters from broadband recordings in Japan: a comparison of three methods. Bull. Seis. Soc. Am. 95, 1346–1358.

Luo, Y., Huang, Z.X., Peng, Y.J., Zheng, Y.J., 2004. A study on SKS wave splitting beneath the China mainland and adjacent regions. Chinese J. Geophys. 47, 916–926.

Mainprice, D., Barruol, G., Ben Ismail, W., 2000. The seismic anisotropy of the Earth's mantle: from single crystal to polycrystal in Earth's deep interior: Mineral Physics and tomography from the atomic to the global scale. AGU, Washington, D.C, pp. 237–264.

Mainprice, D., Silver, P.G., 1993. Interpretation of SKS-waves using samples from the subcontinental lithosphere. Phys. Earth Planet. Int. 78, 257–280.

Mainprice, D., Tommasi, A., Couvy, H., Cordier, P., 2005. Pressure sensitivity of olivine slip systems and seismic anisotropy of Earth's upper mantle. Nature 433, 731–733.

Molnar, P., Tapponnier, P., 1975. Cenozoic tectonics of Asia: Effect of a continental collision. Science 189, 419–425.

Montelli, R., Nolet, G., Dahlen, F.A., Masters, G., 2006. A catalogue of deep mantle plumes: New results from finite-frequency tomography. Geochem. Geophys. Geosyst. 7, Q11007, doi:10.1029/2006GC001248.

Mooney, W.D., Laske, G., Masters, T.G., 1998. CRUST 5.1: A global crustal model at 5° ×5°. J. Geophys. Res. 103, 727–747.

Morita, Y., 2001. The present and furture situation of the OHP Seismic Network: Broadband Seismic Station in Vietnam. In: Abstract of Joint Meeting of Earth and Planetary Science of Japan, pp. 0–001.

Nataf, H.C., Nakanishi, I., Anderson, D.L., 1984. Anisotropy and shear-velocity heterogeneities in the upper mantle. Geophys. Res. Lett. 11, 109–112.

Nicolas, A., Christensen, N.I., 1987. Formation of anisotropy in upper mantle peridotites-A review, in Composition Structure and Dynamics of the Lithosphere-Asthenosphere System. AGU, Washington, D.C, pp. 111–123.

Rangin, C., Le Pichon, X., Mazzotti, S., Pubellier, M., Chamot-Rooke, N., Aurelio, M., Walpersdorf, A., Quebral, R., 1999. Plate convergence measured by GPS across the Sundaland/ Philippine Sea plate deformed boundary: The Philippines and eastern Indonesia. Geophys. J. Int. 139, 296–316.

Restivo, A., Helffrich, G., 1999. Teleseismic shear wave splitting measurements in noisy environments. Geophys. J. Int. 137, 821–830.

Sanderson, D.J., Marchini, W.R.D., 1984. Transpression. J. Structural Geology 6, 449–458.

Sieminski, A., Liu, Q.Y., Trampert, J., Tromp, J., 2007. Finite-frequency sensitivity of body waves to anisotropy based upon adjoint methods. Geophys. J. Int. 168, 1153–1174, doi:10.1111/j.1365-246X.2007.03528.x.

Silver, P.G., 1996. Seismic anisotropy beneath the continents: probing the depths of geology. Annu. Rev. Earth Planet. Sci. 24, 385–432.

Silver, P.G., Chan, W.W., 1991. Shear wave splitting and subcontinental mantle deformation. J. Geophys. Res. 96, 16429–16454.

Silver, P.G., Savage, M.K., 1994. The interpretation of shear-wave splitting parameters in the presence of two anisotropic layers. Geophys. J. Int. 119, 949–963.

Sol, S., Meltzer, A., Burgmann, R., van der Hilst, R.D., King, R., Chen, Z., Koons, P.O., Lev, E., Liu, Y.P., Zeitler, P.K., Zhang, X., Zhang, J., Zurek, B., 2007. Geodynamics of the southeastern Tibetan Plateau from seismic anisotropy and geodesy. Geology 35, 563–566.

Takeuchi, N., Morita, Y., Xuyen, N.D., Zung, N.Q., 2008. Extent of the low-velocity region in the lowermost mantle beneath the western Pacific detected by the Vietnamese broadband seismograph array. Geophys. Res. Lett. 35, L05307, doi:10.1029/2008GL033197.

Tapponnier, P., Pelzer, G., Ledain, A.Y., Armijo, R., Cobbold, P., 1982. Propagating extrusion tectonics in Asia: new insights from simple experiments with plasticine. Geology 10, 611–616.

Thomas, C., Wookey, J., Simpson, M., 2007. D" anisotropy beneath Southeast Asia. Geophys. Res. Lett. 34, doi:10.1029/2006GL02896.

Tu, K., Flower, M.F.J., Carlson, R.W., Zhang, M., Xie, G., 1991. Sr, Nd, and Pb isotopic compositions of Hainan basalts (south China): Implications for a subcontinental lithosphere Dupal source. Geology 19, 567–569.

Vinnik, L.P., Kind, R., Kosarev, G.L., Makeyeva, L.I., 1989. Azimuthal anisotropy in the lithosphere from observation of long -period S-waves. Geophys. J. Int. 99, 549–559.

Vinnik, L.P., Makeyeva, L.I., Milev, A., Usenko, A.Y., 1992. Global patterns of azimuthal anisotropy and deformations in the continental mantle. Geophys. J. Int. 111, 433–447.

Walker, K.T., Bokelmann, G.H.R., Klemperer, S.L., 2004. Shear-wave splitting beneath the Snake River Plain suggests a mantle upwelling beneath eastern Nevada USA. Earth Planet. Sci. Lett. 222, 529–542.

Wang, E., Burchfiel, B.C., Royden, L.H., Chen, L., Chen, J., Li, W., Chen, Z., 1998. Late Cenozoic Xianshuihe-Xiaojiang, Red River, and Dali fault systems of southwestern Sichuan and central Yunnan China. Spec. Pap. Geol. Soc. Am. 327, doi:10.1046/j.1365-3091.2000.0739a.x.

Wang, Q., Zhang, P., Freymueller, J.T., Bilham, R., Larson, K.M., Lai, X., You, X., Niu, Z., Wu, J., Li, Y., Liu, J., Yang, Z., Chen, Q., 2001. Present-day crustal deformation in China constrained by Global Positioning System measurements. Science 294, 574–577.

Wolfe, C.J., Silver, P.G., 1998. Seismic anisotropy of oceanic upper mantle: Shear-wave splitting observations and methodologies. J. Geophy. Res. 103, 749–771.

Wüstefeld, A., Bokelmann, G., 2007. Null detection in shear-wave splitting measurements. Bull. Seis. Soc. Am. 97, 1204–1211.

Zhao, L., Zheng, T.Y., Chen, L., Tang, Q.S., 2007. Shear wave splitting in eastern and Central China: implications for upper mantle deformation beneath continental margin. Phys. Earth Planet. Inter. 162, 73–84.